Audible and Infrasonic waves generated during the 2022 Hunga eruption: Observations from across Aotearoa New Zealand

Oliver D. Lamb[a], Paul Jarvis[b], Geoff Kilgour[a]

[a] *Te Pū Ao - GNS Science, Wairakei Research Centre, Taupō, 3384, New Zealand*
[b] *Te Pū Ao - GNS Science, Avalon Campus, Lower Hutt, 5011, New Zealand*

Abstract

The 15 January 2022 eruption of Hunga volcano (Kingdom of Tonga) featured one of the most powerful blasts in recent history, generating atmospheric acoustic phenomena observed around the world. Here we examine seismo-acoustic data of the eruption from across Aotearoa New Zealand, host of the densest network of seismo-acoustic sensors in the south-west Pacific. We find clear evidence for two wavepackets of audible acoustics generated by the eruption propagating north-to-south across Aotearoa New Zealand. Celerities estimated from manually picked arrival times indicate that each wavepacket was likely induced by nonlinear phenomena during the passage of Lamb and Pekeris waves, the latter an atmospheric resonance mode not observed prior to the eruption of Hunga volcano. We also highlight results from array processing across a large scale acoustic network, where we successfully detect and estimate backazimuths for coherent low frequency acoustic waves across a maximum aperture of 11 km. The observations presented here provide a new dataset for developing novel techniques for modelling and

Email address: o.lamb@gns.cri.nz (Oliver D. Lamb)

monitoring of rare atmospheric acoustic phenomena.

Keywords:
Hunga volcano, Acoustics, Lamb wave, Pekeris wave, Volcano infrasound

1. Introduction

On 15 January 2022, Hunga volcano underwent one of the most explosive eruptions in recent history. The mostly submerged caldera volcano, located in the southwest Pacific, is one of a chain of volcanoes along the Tonga-Kermadec intraoceanic volcanic arc (Cronin et al., 2017; Brenna et al., 2022). The 15 January eruption was the climax of a sequence that began on 19 December 2021 with mostly Surtseyan activity, pyroclastic surges, and sporadic ash plumes rising up to 20 km altitude (Global Volcanism Program, 2022a; Gupta et al., 2022). The main event was preceded by a large explosive eruption on 13 January that generated a 20 km high, 260 km diameter ash plume and removed the middle third of the Hunga Tonga-Hunga Ha'apai island (Global Volcanism Program, 2022b; Gupta et al., 2022). The climactic eruption began at approximately 04:00 UTC on 15 January, producing an ash plume that quickly rose to a height of 57 km with the umbrella cloud reaching a diameter of ∼450 km within 150 minutes (Carr et al., 2022; Gupta et al., 2022; Proud et al., 2022). Underwater volcaniclastic density currents triggered by the eruption travelled >100 km from the volcano at velocities of up to 122 km.hr^{-1} (Clare et al., 2023). The ash plume also featured record-breaking levels of volcanic lightning, reaching peak levels of ∼5000 flashes per minute (Van Eaton et al., 2023; Jarvis et al., 2024). Within the atmosphere, the eruption generated a broad range of intense acoustic waves that were comparable to the 1883 eruption of Krakatau, most prominently a Lamb wave ($<$0.01 Hz) that propagated four times around the world (Matoza et al., 2022). Remarkably, the eruption was also audible at long range distances, with reports from New Zealand ($\sim$1,900 – 3,200 km from Hunga volcano; Lawson et al., 2022, Clive et al. *In Review*), Alaska ($\sim$10,000 km; Matoza et al., 2022), and Germany ($\sim$16,800 km; Kraft et al., 2023). Lastly, a complex and globally observed tsunami was generated by the eruption including air-sea coupling from the large Lamb wave (Carvajal et al., 2022; Gusman et al., 2022; Kubota et al., 2022; Lynett et al., 2022).

Despite the wealth of observations from around the world on the eruption and its effects, there is currently no general consensus on the exact sequence and timing of eruptive activity after 04:00 on 15 January (all times here are reported in UTC, unless otherwise indicated). The relative remoteness of the volcano and intensity of the eruption precluded the possibility of direct visual observations to corroborate the timing of signals in data. On the other hand, the lack of consensus between different datasets may reflect the complexity of the eruption processes that may have occurred during this particularly intense eruption. In general, the key observations were as follows. An eruption plume was first observed in satellite images at 02:57 which briefly rose to a height of 15 km and persisted through to 03:57 (Van Eaton et al., 2023). The main eruption phase began at approximately 04:00 with a gradual increase in eruptive activity as seen in seismic and acoustic data (Matoza et al., 2022; Vergoz et al., 2022; Purkis et al., 2023). An explosion occurred at 04:05-06 which generated the first observed ash plumes over 20 km altitude and generated the first ionospheric disturbance (Astafyeva et al., 2022; Le Bras et al., 2022; Purkis et al., 2023). Seismic and acoustic data points to the peak eruptive activity beginning at approximately 04:15 (Le Bras et al., 2022; Matoza et al., 2022; Podglajen et al., 2022; Poli and Shapiro, 2022; Thurin et al., 2022; Vergoz et al., 2022; Thurin and Tape, 2023), with ionosphere or tsunami observations suggesting a slightly later time of 04:18 (Astafyeva et al., 2022; Purkis et al., 2023). This event coincides with the origin of the globally observed Lamb wave (Matoza et al., 2022). Acoustic and ionospheric data indicate another potential major eruption at or shortly before 04:30 which has been cited as an alternative origin time for the Lamb wave (Astafyeva et al., 2022; Le Bras et al., 2022; Vergoz et al., 2022; Wright et al., 2022; Purkis et al., 2023). Another major event potentially occurred at approximately 04:54 (Astafyeva et al., 2022; Podglajen et al., 2022; Vergoz et al., 2022; Wright et al., 2022), with observations suggesting this generated the largest near-field tsunami waves in the entire sequence (Purkis et al., 2023). Several smaller eruptions were detected after 05:00 (Le Bras et al., 2022; Vergoz et al., 2022; Wright et al., 2022) with the last eruptive activity on 15 January detected several hours later at approximately 08:25 (Le Bras et al., 2022; Matoza et al., 2022; Podglajen et al., 2022). Note that this description is an approximation of what is described in the literature, with some timelines including multiple subevents (e.g. Le Bras et al., 2022, describe 12 events from 03:40 to 05:30); a summary of the complexity and disagreements of event timing between different data streams is provided in supplementary Figure S1.

Here we present seismic and acoustic observations of the 15 January eruption from across Aotearoa New Zealand (NZ), at distances of 2000 to 3200 km from the volcano. The dataset is notable for being the densest geophysical monitoring network in the southwest Pacific region, with high-quality, high-sampling rate seismo-acoustic data giving us a detailed view of atmospheric acoustic waves propagating north to south across both islands (Fig. 1). We use these data to search for evidence of rare acoustic phenomena induced by the eruption, including the propagation of a previously unobserved Pekeris wave.

2. Data and Methods

2.1. Data

We analyse data from GeoNet, NZ's national monitoring programme run by GNS Science; the network collects a wide range of data to monitor and respond to natural hazards such as volcanoes, landslides, earthquakes, and tsunamis (e.g., Petersen et al., 2011). Seismic data was recorded by a network of short-period and broadband seismometers (Fig. 1; GNS Science, 2021), as well as an extensive network of strong-motion accelerometers (Fig. S2; GNS Science, 2020). Acoustic data was recorded by 22 microphones or barometers deployed near actively monitored volcanoes on the North Island as well as Rangitāhua (Fig. 1; GNS Science, 2022). All seismometers and acoustic sensors recorded data at 100 samples per second, whereas strong-motion accelerometers recorded at 200 samples per second. GeoNet acoustic sensors are usually equipped with mechanical filters to systematically remove frequencies >20 Hz which are typically due to noise from wind or anthropogenic sources.

To help track the 15 January eruption atmospheric acoustics propagating

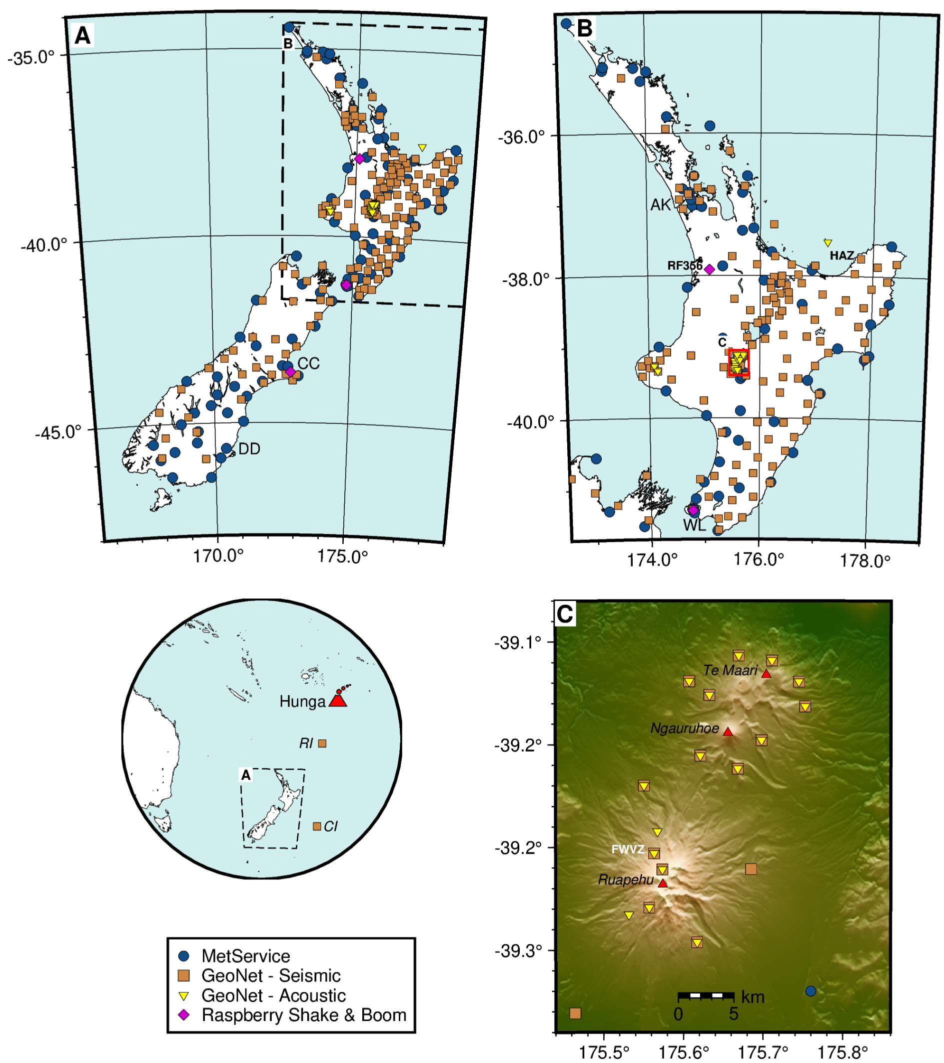

Figure 1: (A) Map of NZ with locations of all stations used in this study. Also marked are locations of major urban areas, AK: Auckland, WL: Wellington, CC: Christchurch, and DD: Dunedin. Inset map below panel A shows location of NZ relative to Hunga volcano (red marker), as well as stations on Rangitāhua (Raoul Island, RI) and Rēkohu (Chatham Island, CI), which also include MetService stations. (B) Zoomed-in map of the North Island within region marked by dashed lines in panel A. Red box marks region plotted in panel C. (C) Map of Tongariro National Park region showing distribution of stations in the area. Also noted are locations of historical eruptions in the area (red triangles; Ngauruhoe, Ruapehu, Te Maari). Locations of stations used in Figs. 2 and 4 are noted in panels B and C. Locations of strong-motion stations are plotted in Fig. S2.

across NZ, we also looked at measurements from two other networks. The first is pressure data from weather stations operated by the national weather authority, the Meteorological Service of New Zealand Ltd., Te Ratonga Tirorangi (MetService). The Vaisala barometer at each station recorded atmospheric pressure at 1 minute intervals, providing a good reference point for the arrival time of the eruption Lamb wave across the country. We also used seismic and acoustic data from the Raspberry Shake network (Fig. 1; Raspberry Shake, S.A., 2016). We focused on three Raspberry Shake and Boom (RS&B) stations that were recording on 15 January, as the co-located seismic and acoustic sensors were useful for interpreting signals at audible frequencies (>20 Hz); each Raspberry Shake and Boom sensor package records data at 100 samples per second.

2.2. Methods

To provide more insights into the chronology of the 15 January Hunga eruption sequence we applied array processing to acoustic data recorded by GeoNet sensors. Traditionally, acoustic array processing was only applied to sensors separated by distances of 10s to 100s of metres as they targeted coherent arrivals with wavelengths of a similar magnitude (e.g., Ripepe and Marchetti, 2002; Matoza et al., 2007; Fee et al., 2010). Lamb waves dominate at frequencies <0.01 Hz, which equates to wavelengths of >30 km. Therefore, for our array processing we considered the GeoNet network of 9 acoustic sensors around the Tongariro and Ngauruhoe volcanoes as one array (maximum aperture of 11 km and elevation difference of 418 m; Fig. 1c). We applied the Narrow-Band Least-Squares array processing approach (Iezzi et al., 2022) to acoustic data recorded from 03:45 to 13:00 on 15 January, bandpass filtered from 0.001 to 0.25 Hz. Processing was conducted across 8 frequency bands, with time windows ranging from 2400 to 180 s for lower to higher frequency bands (see Table S1 for details). Coherent signals travelling across the Tongariro-Ngauruhoe network were identified using Median Cross-Correlation Maxima (MdCCM) >0.7 and σ_τ <1; σ_τ is an indicator of nonplanar propagation across an array (Szuberla et al., 2006).

We applied a short-term average/long-term average (STA/LTA) algorithm (Allen, 1978) to help quantify the characteristics of air-to-ground coupled audible booms recorded via seismic data. We took advantage of GeoNet sites with co-located seismometers and strong-motion accelerometers (Fig. 4d, e, S3), where STA/LTA "picks" on both sensors were more likely to be real instead of false positives. Using a recursive STA/LTA algorithm (Withers et al., 1998) with 2 and 6 second short- and long-term windows, we used a threshold of 1.6 in the resulting characteristics function to define a pick; picks detected simultaneously by the seismometer and strong-motion accelerometer were kept as detections. This analysis was conducted at 43 sites across NZ, with data from each sensor highpass filtered at 20 Hz.

3. Results

3.1. Acoustic observations and analysis

Acoustic waves from the 15 January Hunga eruption were well recorded across NZ (Fig. 2a) and were dominated by the large amplitude Lamb wave (604 Pa peak-to-peak pressure difference; Fig. 2d, e). The Lamb wave appears similar at all MetService and GeoNet acoustic stations, with a total duration of approximately 90 minutes (Fig. 2d). Manual picking of the onset time of the Lamb wave at each MetService and GeoNet station gives a celerity of 313 m.s^{-1} (black dotted line in Fig. 2a) with a backprojected origin time at Hunga of 04:15, assuming a constant celerity. In contrast, the three RS&B sensors could not capture the Lamb wave as they are not sensitive to frequencies less than 1 Hz (Fig. 2a - c). However, unlike the GeoNet and MetService sensors, they are sensitive to frequencies at 20 – 50 Hz due to their higher sampling rate or lack of mechanical filters. Each RS&B sensor records two distinct clusters of arrivals at frequencies >1 Hz, with some arrivals extending into the audible range (>20 Hz; Fig. 2b, c). Henceforth, we distinguish each high frequency cluster as Wavepackets 1 and 2. We also observed an increase in acoustic energies that began approximately 15 minutes before the apparent arrival of the Lamb wave (Fig. 2b).

Array processing of GeoNet acoustic data across the Tongariro-Ngauruhoe network found coherent arrivals from 06:00 to 08:00, as well as a later arrival at 10:30 to 11:00 (Fig. 3). We also observed coherent arrivals up to 15 minutes before the apparent arrival of the Lamb wave (black dotted line in Fig. 3b). Backazimuths for all coherent arrivals were mostly centred at approximately 25°, which corresponds to the backazimuth towards Hunga volcano from Tongariro-Ngauruhoe volcanoes (Fig. 3c). Trace velocities for both arrivals were within 300 – 350 m.s^{-1}, with higher frequencies correlating with higher trace velocities (Fig. 3d). We also noted a significant decrease in trace velocities during the first arrival at approximately 06:45 - 07:10; the lowest value was 295 m.s^{-1} at 07:05.

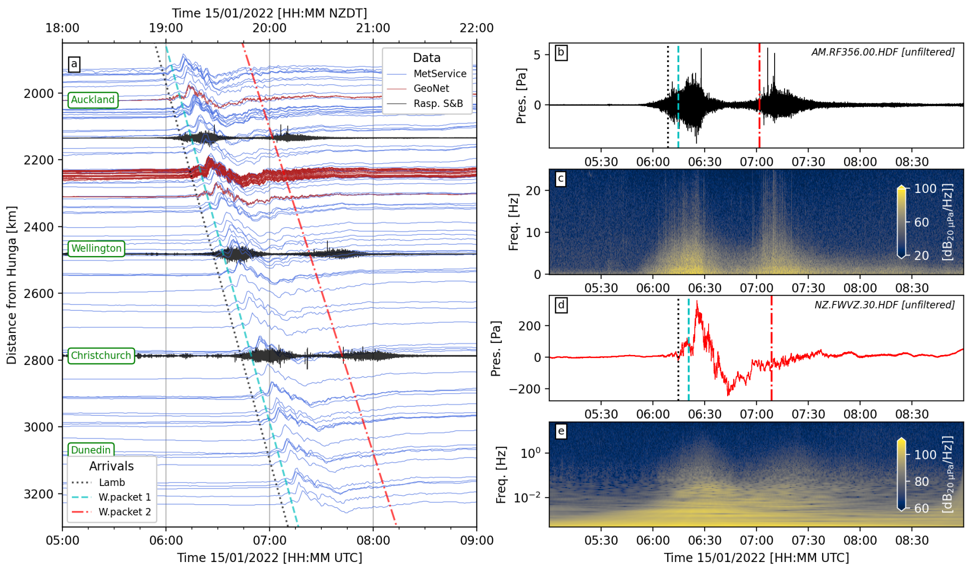

Figure 2: (a) Unfiltered atmospheric acoustic data recorded across NZ after the Hunga eruption on 15 January 2022. Also plotted are arrival times for the Lamb wave (black dotted line), and audible wavepackets 1 and 2 (cyan dashed and red dot-dash line), and distances of major cities in NZ. (b) Unfiltered acoustic data recorded by a Raspberry Shake and Boom station (RF356). (c) Frequency spectrogram of acoustic data recorded by RF356. (d) Unfiltered acoustic data recorded at a GeoNet acoustic sensor (FWVZ). (e) Continuous wavelet transform frequency spectrogram of acoustic data recorded at FWVZ.

3.2. Seismic observations and analysis

GeoNet acoustic stations were designed to monitor for eruptive activity so were exclusively deployed in close proximity to volcanoes in the North Island (Fig. 1). As a result, the GeoNet acoustic sensors can only provide a limited view the Hunga eruption acoustic wavefield as it travelled over NZ. Seismic sensors commonly record ground-coupled airwaves, where incident atmospheric acoustic waves impinge on the earth surface and is par-

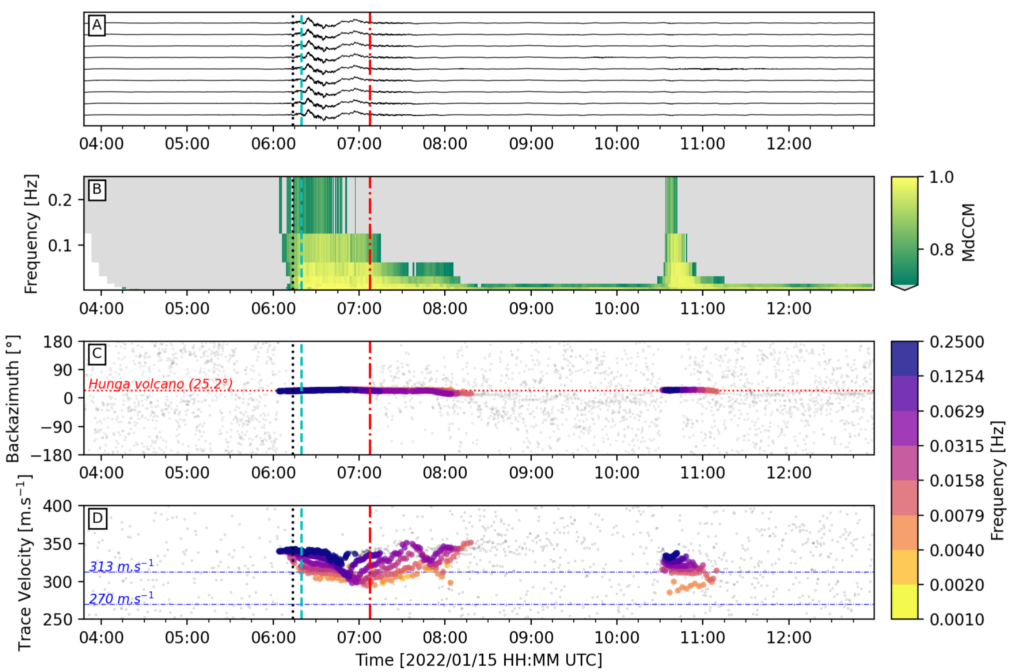

Figure 3: Results of array processing using microphones around the Tongariro-Ngauruhoe volcanoes. (A) Acoustic data as recorded by the stations used in the array processing, bandpass filtered at 0.001 to 0.25 Hz. (B) MdCCM for each time window and frequency band; estimations below the 0.7 threshold are coloured in grey. Each estimate is plotted at the end of their respective time window. (C) Back-azimuth and (D) Trace velocity estimates for MdCCM >0.7 and σ_τ <1, coloured by frequency. Estimates which fall outside those thresholds are plotted as grey dots.

tially transmitted as a seismic wave (e.g., Arrowsmith et al., 2010; McKee et al., 2018; Dannemann Dugick et al., 2023). Therefore, we explored seismic data recorded by GeoNet broadband, short-period, and strong-motion sensors from across NZ (Fig. 1, S2) to track the passage of audible waves via ground-coupled airwaves.

After applying a highpass filter at 20 Hz, seismic data from across NZ clearly record the clusters of arrivals we previously labelled as Wavepackets 1 and 2 (Fig. 4a-c, S3). To estimate the celerity of each wavepacket, we manually picked their apparent arrival times at 27 seismic stations across the country. We find that Wavepacket 1 had a celerity of 313 $m.s^{-1}$, whereas for Wavepacket 2 it was 270 $m.s^{-1}$ (Fig. 5). Assuming a constant celerity, extrapolation back to the origin at Hunga volcano finds origin times of 04:21 and 04:50 for Wavepackets 1 and 2, respectively.

The number of detections found at each site analysed varied widely, ranging from 2 to 238 (Fig. 6a). This was most likely due to local noise or site conditions affecting signal-to-noise ratios or introducing non-natural signals at each site. To extract picks related to the Hunga eruption wavepackets, we excluded picks outside of two 30 minute time windows based on expected arrival times calculated from the previously estimated celerities (Fig. 5, 6a); the time windows start 5 minutes before each expected arrival. Detections within each time window ranged from 1 to 96, with a median of 39. We find that the number of detections was generally greater in Wavepacket 2 versus Wavepacket 1 (Fig. 6b, c). Using data in a 2 s window centred on each detection, we also tracked seismic amplitudes at each station. We find that median seismic amplitudes for detections decrease from north to south (Fig. 6d). Furthermore, we also observed that median seismic amplitudes for detections in Wavepacket 2 were generally larger than those in Wavepacket 1 (Fig. 6e, f). However, the median seismic amplitudes for Wavepacket 2 appear to decrease faster than Wavepacket 1 as the latter had higher values in the south of NZ compared to the north (Fig. 6f).

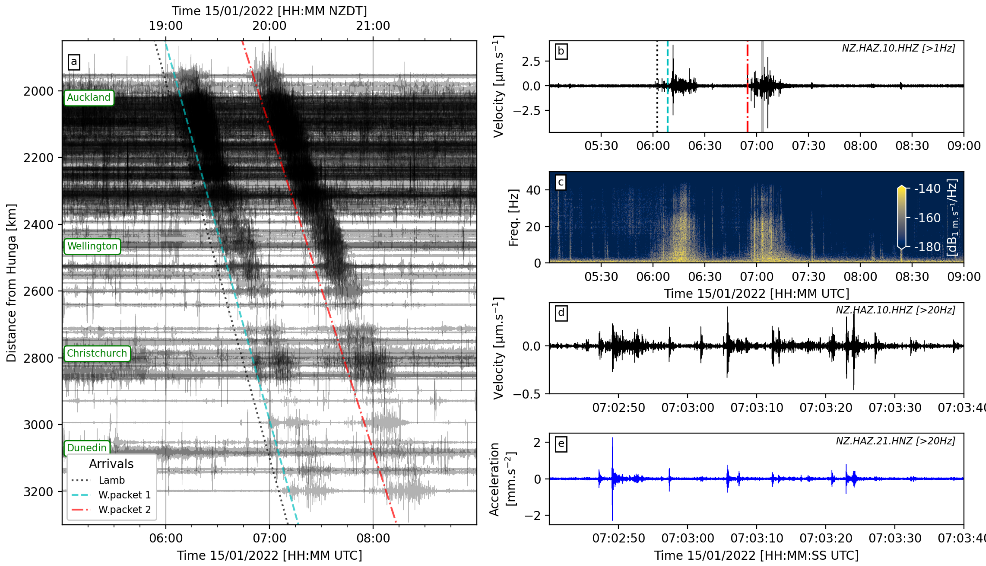

Figure 4: (a) Seismic data recorded across NZ after the Hunga eruption on 15 January 2022, highpass filtered at 20 Hz. Also plotted are arrival times for the Lamb wave (black dotted line), and audible wavepackets 1 and 2 (cyan dashed and red dot-dash line), and distances of major cities in NZ. (b) Seismic data recorded by GeoNet broadband seismometer HAZ, highpass filtered at 1 Hz. Gray area marks timespan of data plotted in panels d and e. (c) Frequency spectrogram of seismic data recorded at HAZ. (d) Clip of seismic data recorded at HAZ, highpass filtered at 20 Hz, during timepsan marked by grey area in panel b. (e) Clip of strong-motion accelerometer data recorded at HAZ, during same time as panel d.

4. Discussion

The seismo-acoustic data recorded across NZ provides a unique view into the unprecedented eruption of Hunga volcano on 15 January 2022. The observation of two separate wavepackets of ground-coupled audible waves from the eruption has not been previously described and may in turn provide new insights into the chronology of events during the peak phase of eruptive

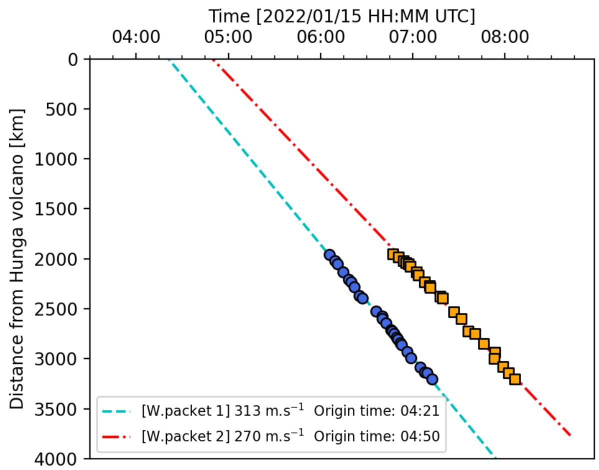

Figure 5: Picked arrival times for wavepackets 1 and 2, as well as interpolated linear relationships showing velocities and origin times at Hunga volcano.

activity on 15 January. We have divided our interpretations of the data into three parts: the first addresses the origin of the audible waves generated by the eruption, the second outlines the implications our observations may have for the activity timeline at Hunga volcano, and the third briefly examines the array processing conducted here.

4.1. Source of audible acoustics

The nationwide occurrence of audible acoustic signals was an unprecedented phenomenon prior to the eruption of Hunga volcano on 15 January 2022 (Lawson et al., 2022). Only the 1883 eruption of Krakatau provided any kind of precedent for long-range audible acoustics from volcanoes (Strachey, 1888). Previous studies had observed only one wavepacket of audible signals (Matoza et al., 2022; Kraft et al., 2023) but we show clear evidence for two wavepackets generated by the Hunga eruption (Figs. 2, 4). Based

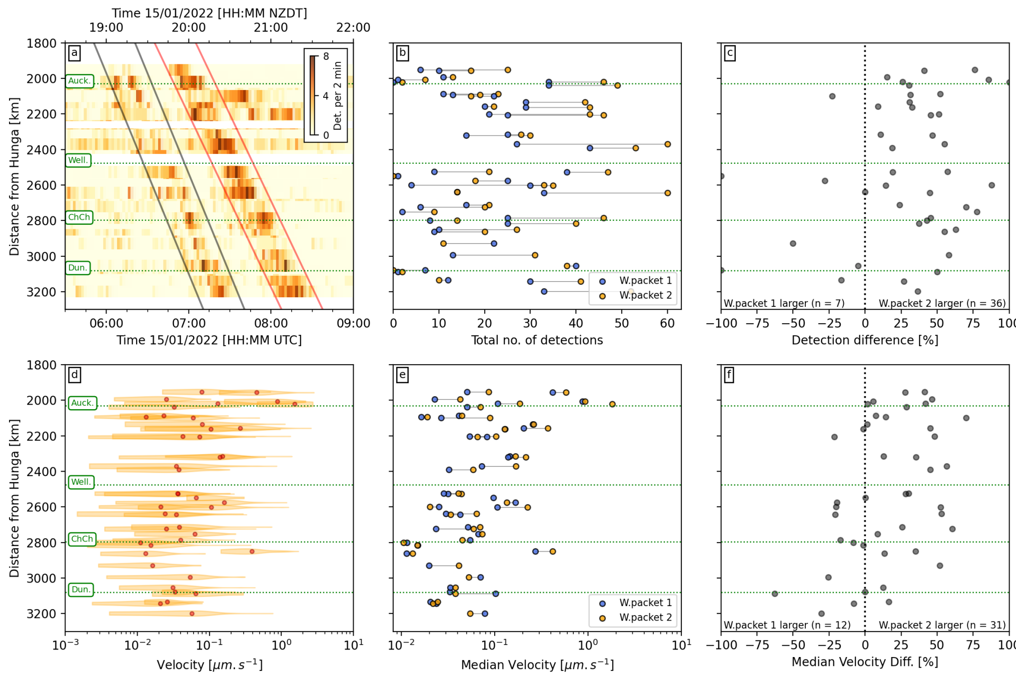

Figure 6: Results of detection analysis on co-deployed broadband and strong-motion seismic sensors. (a) Detections per 2 minute window at each site, where colour indicates the total number of detections within each window. Lines indicate windows used to delineate wavepackets 1 and 2. (b) Number of detections within wavepacket 1 (blue dots) versus wavepacket 2 (orange dots) for each station (connected by lines). (c) Comparison of total detections within each wavepacket, where +/- percentiles indicate greater detections in wavepacket 2/1, respectively. (d) Violin plots showing distribution of maximum seismic amplitudes of each detection at each station. Median values are plotted with red circles. (e) Median maximum seismic amplitudes for detections with Wavepacket 1 (blue circles) and Wavepacket 2 (orange circles) for each station (connected by lines). (f) Similar to panel c, but comparing differences in median maximum seismic amplitudes within each wavepacket.

on arrival times of each wavepacket across NZ (Fig. 5), Wavepacket 1 had a higher celerity (313 m.s^{-1}) than Wavepacket 2 (270 m.s^{-1}). The celerity for the first wavepacket corresponded closely with previously estimated values for the Hunga eruption Lamb wave (312 – 319 $m.s^{-1}$; Matoza et al., 2022; Kraft et al., 2023; Jarvis et al., 2024), therefore we associate Wavepacket 1 with the passage of the Lamb wave over NZ. In contrast, few studies have reported any atmospheric phenomena with celerities that correspond with that of Wavepacket 2. Matoza et al. (2022) report infrasonic arrivals for a continuous ∼2 hour period after the Lamb waves with group velocities ranging from 250 to 290 $m.s^{-1}$. Watanabe et al. (2022) used satellite radiance observations to describe an atmospheric resonance mode with a phase speed of 270 $m.s^{-1}$ south of Hunga volcano. This resonance mode, now called the Pekeris wave, had never been previously directly observed since it was originally theorised in 1937 (Pekeris, 1937). Considering the distinct 30-45 minute length of Wavepacket 2 and the close match in celerity with satellite observations, we consider the Pekeris wave a strong candidate for generating the second group of audible atmospheric acoustics across NZ. It is notable that the arrival of the Pekeris wave was not clearly recorded in the GeoNet and Metservice sensors, despite clearly recording the preceding Lamb wave (Fig. 2a, d). However, the Pekeris wave was found to have an amplitude structure that, relative to the Lamb wave, is amplified in the stratosphere and mesosphere relative to the troposphere (see Fig. 8 in Watanabe et al., 2022); this was confirmed via comparing measurements of the upper ionosphere with ground level atmospheric pressure in Japan (Ohya et al., 2024).

Two hypotheses have thus far been proposed for generating the audible acoustics heard at global distances: the intense volcanic lightning activity observed at Hunga volcano during and after the eruption (Kraft et al., 2023), or nonlinear energy cascades from lower to audible frequencies (Matoza et al., 2022). Record levels of volcanic lightning activity were observed for up to 3 hours after the main eruption at ∼04:00 on 15 January 2022; further lightning activity was observed during a later eruptive phase at 08:25 (Van Eaton et al., 2023; Bór et al., 2023; Jarvis et al., 2024). A key observation was that the lightning activity was occurring continuously after the main eruption, which cannot explain the two distinct audible Wavepackets observed across NZ (Figs. 2, 4). Furthermore, if both Wavepackets were generated by the lightning then we would expect their celerities to match which was not what we observed (Fig. 5). Therefore, we rule out volcanic lightning generated by the Hunga eruption as a source for the global audible acoustics observed in NZ, Alaska, and Germany.

The generation of audible acoustics by volcanic eruptions at long-range distances (hundreds to thousands of kms) via nonlinear energy cascades was originally proposed after the 1980 eruption of Mount St Helens (Reed, 1987). We note that this phenomenon differs from the more commonly observed acoustic shockwaves generated at the source (i.e., the eruption vent) which decay rapidly and therefore are only recorded by sensors within a few kilometres of the volcano (Dragoni and Santoro, 2020). For longer distances, it was hypothesised that acoustic waves travelling into higher altitudes (>50 km) form shockwaves which are then refracted back to ground level (Reed, 1987). Recent studies have successfully modelled shockwaves in the upper atmosphere from nonlinear evolution of low frequency acoustic waves induced by tectonic earthquakes (Nozuka et al., 2024). However, these shockwaves were only detectable in Global Navigation Satellite System Total Electron Content observations as the shockwaves do not refract back to ground-level. As far as we are aware, no model currently exists that can account for ground-level observations of audible acoustic waves generated in the upper atmosphere. We put forward that the dataset described here will provide a benchmark upon which future modelling efforts can be tested against. The new models will need to account for three key observations: i) audible waves were generated not only by the Lamb wave, but also the Pekeris wave, ii) audible waves arrived 6 minutes after the onset of the Lamb wave, and iii) why audible waves generated by the Pekeris were apparently more numerous and louder than those generated by the Lamb wave (Fig. 6).

4.2. Insights towards Hunga eruption chronology

The complex sequence of activity at Hunga volcano on 15 January 2022 and the remoteness of the volcano has resulted in a general lack of consensus between different datasets regarding the eruption chronology and the driving processes behind them. While the seismo-acoustic data and observations presented here cannot provide an unequivocal eruptive sequence, our results help illuminate the processes that may have occurred during the eruption. We focus on two key observations in the seismo-acoustic dataset: i) the origin of the Lamb wave and the acoustic activity preceding it, and ii) the source of the Pekeris wave.

Assuming a constant celerity, the Lamb waves originated at 04:15 at Hunga volcano (Fig. 2a). This coincides closely with the timing of the most energetic seismo-acoustic activity, a tsunami, and ionospheric disturbances (e.g. Astafyeva et al., 2022; Le Bras et al., 2022; Matoza et al., 2022; Podglajen et al., 2022; Thurin et al., 2022; Purkis et al., 2023). This arrival time is also sooner than an apparent event at 04:30 which was previously hypothesised to have generated the Lamb wave (Astafyeva et al., 2022; Le Bras et al., 2022; Vergoz et al., 2022; Wright et al., 2022; Purkis et al., 2023). While our evidence is not conclusive and we have assumed a constant celerity, our observations suggest that the 04:15 event was the origin for the Lamb wave. Infrasonic waves were observed up to 15 minutes before the arrival of the Lamb wave which suggests an earlier time for the onset of the eruptive activity on 15 January (Fig. 2b). Multiple studies across different disciplines have identified a period from 04:00 to 04:06 as the onset time for the activity at Hunga volcano (Vergoz et al., 2022; Matoza et al., 2022; Gupta et al., 2022; Astafyeva et al., 2022). However, it must be noted that the acoustic arrivals observed here have an emergent arrival, where an arrival time can only be defined above a certain signal-to-noise ratio; this suggests that the onset time of the activity may be earlier than 04:00. Weak infrasonic signals were detected from Hunga volcano (albeit with large location errors) originating at 03:46 (Le Bras et al., 2022; Matoza et al., 2022). An eruption plume was observed as early as 02:57 and persisted through to 03:57 (Van Eaton et al., 2023), suggesting the infrasonic activity preceding the Lamb wave was due to relatively low-level eruptive activity before the main eruption at 04:15. It was only once the main eruptive phase began at 04:00 - 04:06 was the activity energetic enough to generate acoustic waves detectable at long-range distances.

The origin of the Pekeris wave may be more enigmatic as it's arrival time was derived from seismic data recorded across NZ (Figs. 4, 5). Our arrival time picks suggest an origin time at Hunga volcano of 04:50 but if we assume the same source process as the Lamb wave-generated audible waves (see previous section) and note that the Lamb wave arrival preceded Wavepacket 1 by 6 minutes (Fig. 2a) then the origin time of the Pekeris wave may in fact be as early as 04:44. There were several notable observations around this time period in the eruption: major seismic events were detected at 04:30, 04:36 and 04:40 (Kintner et al., 2022; Matoza et al., 2022; Le Bras et al., 2022), a major ionospheric event originated at 04:43 (Astafyeva et al., 2022), an acoustic event was detected at 04:53 (Podglajen et al., 2022), and a large tsunami originated at the volcano at 04:56 (Purkis et al., 2023). Altogether, this suggests that a major explosive event occurred at Hunga volcano between 04:40 to 04:56 and may be the source of the Pekeris wave observed in this study. However, we also note that shortly after the ash plume reached the mesosphere (>50 km) at 04:36 it collapsed down to 40 km at 04:47 before rising again up to 58 km 04:57 (Proud et al., 2022; Van Eaton et al., 2023; Jarvis et al., 2024). This is approximately the same altitude where the Pekeris wave was found to be amplified relative to lower altitudes (Watanabe et al., 2022; Ohya et al., 2024). Later tsunami phases induced by the Hunga eruption have also been linked to the propagation of the Pekeris wave (Fujii and Satake, 2024). Therefore we propose an alternative hypothesis for the origin of the Pekeris wave: the interaction of the fast-ascending ash plume with the upper stratosphere and lower mesophere. In other words, we propose that the extremely rapid insertion and temporary collapse of a water-rich ash plume at 40 – 60 km altitudes was sufficient to induce a large scale atmospheric oscillation that was transmitted as a Pekeris wave. This process may help explain the apparent separation in time between the seismic events at 04:30 to 04:40 and the acoustic and tsunami events after 04:50, where the seismicity was due to activity at or below the vent with no measurable impact on the ash plume or atmosphere. Modelling of a 50 km high ash plume containing 90% steam found mass ascent velocities of >200 m.s^{-1} at up to 40 km altitude (Mastin et al., 2024). However, careful atmospheric modelling is required to assess whether this high ascent velocity combined with the erupted ash plume mass is enough to induce Pekeris waves in the atmosphere, therefore we cannot conclusively deduce how the Pekeris wave was generated during the Hunga eruption.

4.3. Large aperture array processing

Our novel array processing method using a large aperture (11 km) network successfully estimated back-azimuth directions of low frequency signals such as Lamb waves (<0.25 Hz; Fig. 3). We find coherent detections across all frequency bands between 0.001 to 0.25 Hz during our analysis time span, with two separate arrivals originating from the direction of Hunga volcano. Trace velocities within the first arrival were broadly consistent with Lamb wave velocities (300 – 350 m.s^{-1}), with the noteworthy decrease to <300 m.s^{-1} coinciding with the arrival of the Pekeris wave. The second arrival from 10:30 to 11:00 likely originates from the last eruptive activity detected at Hunga volcano on 15 January, several hours after the main eruption (Le Bras et al., 2022; Matoza et al., 2022; Podglajen et al., 2022). As far as we are aware, with a maximum inter-station distance of 11 km this is the largest aperture network of atmospheric acoustic sensors used as an array for detecting signals from a volcanic eruption.

To help quantify the sensitivity of this network array to detecting remote volcanic activity, we expanded our analysis to assess if less energetic eruptive activity observed at Hunga volcano on 13-14 January was also detected (Global Volcanism Program, 2022b; Gupta et al., 2022; Vergoz et al., 2022). Activity during this period was characterised by an eruption that began at 15:20 on 13 January and continued until 18:00 on 14 January (Vergoz et al., 2022), generating a 18 km high plume (Gupta et al., 2022), as well as a small tsunami (Global Volcanism Program, 2022b). Array analysis over this time period does not detect any coherent signals except for 3 or 4 low-frequency arrivals during a four hour period from 08:00 to 12:00 on 14 January, with estimated back-azimuths towards Hunga volcano (Figs. S5, S6). This period coincides with reduced infrasonic intensity but preceded increased hydroacoustic intensity as observed at International Monitoring System stations (Vergoz et al., 2022). Observed plume heights during this eruptive phase were oscillating, suggesting the occurrence of multiple explosions during an unsteady eruption (Gupta et al., 2022). It is not immediately clear why the network array failed to detect the most intense acoustic acoustics on 13 January, but we hypothesise that atmospheric conditions were not favourable for the propagation of acoustic waves from the earliest stages of this eruptive phase. Nevertheless, the detection of multiple arrivals on 14 January coinciding with infrasonic and hydroacoustic detections suggests the occurrence of a major eruptive event during this phase of activity. We suggest this could be linked to the collapse of the caldera rim between the islands of Hunga Ha'apai and Hunga Tonga, as detected by satellite images (Global Volcanism Program, 2022b). Altogether, these array processing results suggest the network array was only sensitive to large, sub-Plinian or Plinian sized eruptions (VEI≥3) across the south-west Pacific and further afield. In general, these results demonstrate how a large scale array of acoustic sensors could be used to detect large scale volcanic eruptions across the SW Pacific, as well as other sources of low frequency acoustics such as meteors, tectonic earthquakes, tsunamis, and human-induced explosions (Le Pichon et al., 2019, and references therein).

5. Conclusions

Here we present an overview of seismo-acoustic observations of the 15 January 2022 eruption of Hunga volcano as recorded across NZ, with a focus on the passage of atmospheric acoustic waves across the country. The results help illustrate the timing of eruptive activity at the volcano as well as rare atmospheric resonance phenomena induced by the activity. We observed infrasonic arrivals from Hunga volcano for at least 15 minutes prior to the arrival of the Lamb wave, suggesting the main eruptive phase of the 15 January eruption began at or shortly before 04:00. We find evidence for two wavepackets of audible acoustics generated by the eruption and recorded across all of NZ. Celerities estimated from arrival times indicate that each wavepacket was likely induced by nonlinear phenomena during the passage of Lamb and Pekeris waves, the latter an atmospheric resonance mode not observed prior to the eruption of Hunga volcano. The source process of the Pekeris wave is unclear with timing suggesting either a second large explosion after the main eruption at 04:15, or atmospheric resonance induced by the injection of an ash plume to mesopheric altitudes. We also highlight results from array processing across a large scale acoustic network near volcanoes in central NZ, where we successfully detect and estimate backazimuths for coherent acoustic waves across a maximum aperture of 11 km. We conclude that the results presented here can provide a new dataset to help the development of new techniques for modelling and monitoring of rare atmospheric acoustic phenomena.

6. Funding

This work was supported by the New Zealand Ministry of Business, Innovation and Employment (MBIE) through the Hazards and Risk Management Programme (Strategic Science Investment Fund, contract CO5X1702).

7. Data availability

The GeoNet seismic and acoustic data analysed in this study are available for download via the GeoNet FDSN web service (https://www.geonet.org.nz/data/access/FDSN). Raspberry Shake and Boom data are available to download via the IRIS-DMC (https://ds.iris.edu/mda/AM/). MetService data are available on request (https://about.metservice.com/our-company/about-this-site/open-access-data/).

8. Acknowledgements

This manuscript benefited greatly from various Python packages, including Obspy (Krischer et al., 2015), Matplotlib (Hunter, 2007), and PyGMT (Uieda et al., 2023). We also thank Chris Noble at MetService for providing the MetService data.

9. Author contributions

Conceptualization: all authors; Investigation: O.D.L.; Visualization: O.D.L.; Writing - original draft: O.D.L.; Writing - review & editing: all authors.

References

Allen, R.V., 1978. Automatic earthquake recognition and timing from single traces. Bulletin of the Seismological Society of America 68, 1521–1532.

Arrowsmith, S.J., Johnson, J.B., Drob, D.P., Hedlin, M.A., 2010. The seismoacoustic wavefield: A new paradigm in studying geophysical phenomena. Reviews of Geophysics 48, 1–23. doi:10.1029/2010RG000335.

Astafyeva, E., Maletckii, B., Mikesell, T.D., Munaibari, E., Ravanelli, M., Coisson, P., Manta, F., Rolland, L., 2022. The 15 January 2022 Hunga Tonga Eruption History as Inferred From Ionospheric Observations. Geophysical Research Letters 49. doi:10.1029/2022GL098827.

Brenna, M., Cronin, S.J., Smith, I.E., Pontesilli, A., Tost, M., Barker, S., Tonga'onevai, S., Kula, T., Vaiomounga, R., 2022. Post-caldera volcanism reveals shallow priming of an intra-ocean arc andesitic caldera: Hunga volcano, Tonga, SW Pacific. Lithos 412–413, 106614. doi:10.1016/j.lithos.2022.106614.

Bór, J., Bozóki, T., Sátori, G., Williams, E., Behnke, S.A., Rycroft, M.J., Buzás, A., Silva, H.G., Kubicki, M., Said, R., Vagasky, C., Steinbach, P., André, K.S., Atkinson, M., 2023. Responses of the AC/DC Global Electric Circuit to Volcanic Electrical Activity in the Hunga Tonga-Hunga

Ha'apai Eruption on 15 January 2022. Journal of Geophysical Research: Atmospheres 128, e2022JD038238. doi:10.1029/2022JD038238.

Carr, J.L., Horváth, A., Wu, D.L., Friberg, M.D., 2022. Stereo Plume Height and Motion Retrievals for the Record-Setting Hunga Tonga-Hunga Ha'apai Eruption of 15 January 2022. Geophysical Research Letters 49. doi:10.1029/2022GL098131.

Carvajal, M., Sepúlveda, I., Gubler, A., Garreaud, R., 2022. Worldwide Signature of the 2022 Tonga Volcanic Tsunami. Geophysical Research Letters 49, e2022GL098153. doi:10.1029/2022GL098153.

Clare, M.A., Yeo, I.A., Watson, S., Wysoczanski, R., Seabrook, S., Mackay, K., Hunt, J.E., Lane, E., Talling, P.J., Pope, E., Cronin, S., Ribó, M., Kula, T., Tappin, D., Henrys, S., de Ronde, C., Urlaub, M., Kutterolf, S., Fonua, S., Panuve, S., Veverka, D., Rapp, R., Kamalov, V., Williams, M., 2023. Fast and destructive density currents created by ocean-entering volcanic eruptions. Science 381. URL: https://www.science.org/doi/10.1126/science.adi3038, doi:10.1126/science.adi3038.

Cronin, S., Brenna, M., Smith, I., Barker, S., Tost, M., Ford, M., Tonga'onevai, S., Kula, T., Vaiomounga, R., 2017. New volcanic island unveils explosive past. Eos doi:10.1029/2017EO076589.

Dannemann Dugick, F., Koch, C., Berg, E., Arrowsmith, S., Albert, S., 2023. A new decade in seismoacoustics (2010–2022). Bulletin of the Seismological Society of America doi:10.1785/0120220157.

Dragoni, M., Santoro, D., 2020. A model for the atmospheric shock wave produced by a strong volcanic explosion. Geophysical Journal International 222, 735–742. doi:10.1093/gji/ggaa205.

Fee, D., Steffke, A., Garcés, M.A., 2010. Characterization of the 2008 Kasatochi and Okmok eruptions using remote infrasound arrays. Journal of Geophysical Research Atmospheres 115, 1–15. doi:10.1029/2009JD013621.

Fujii, Y., Satake, K., 2024. Modeling the 2022 Tonga Eruption Tsunami Recorded on Ocean Bottom Pressure and Tide Gauges Around the Pacific. Pure and Applied Geophysics doi:10.1007/s00024-024-03477-1.

Global Volcanism Program, 2022a. Report on Hunga Tonga-Hunga Ha'apai (Tonga) - February 2022. Bulletin of the Global Volcanism Network 47. URL: https://volcano.si.edu/showreport.cfm?doi=10.5479/si.GVP.BGVN202202-243040, doi:10.5479/si.GVP.BGVN202202-243040.

Global Volcanism Program, 2022b. Report on Hunga Tonga-Hunga Ha'apai (Tonga) - March 2022. Bulletin of the Global Volcanism Network 47. URL: https://volcano.si.edu/showreport.cfm?doi=10.5479/si.GVP.BGVN202203-243040, doi:10.5479/si.GVP.BGVN202203-243040.

GNS Science, 2020. GeoNet Aotearoa New Zealand Strong Motion Data Products. URL: https://data.gns.cri.nz/metadata/srv/eng/catalog.search/metadata/25c52e65-dbf9-4 doi:10.21420/X0MD-MV58.

GNS Science, 2021. GeoNet Aotearoa New Zealand Seismic Digital Waveform Dataset. URL: https://data.gns.cri.nz/metadata/srv/eng/catalog.search/metadata/bebbffb4-4335-4 doi:10.21420/G19Y-9D40.

GNS Science, 2022. GeoNet Aotearoa New Zealand Acoustic Digital Waveform Dataset. URL: https://data.gns.cri.nz/metadata/srv/eng/catalog.search/metadata/e5d1a989-3bf5-4 doi:10.21420/0PRR-YT69.

Gupta, A.K., Bennartz, R., Fauria, K.E., Mittal, T., 2022. Eruption chronology of the December 2021 to January 2022 Hunga Tonga-Hunga Ha'apai eruption sequence. Communications Earth Environment 3, 314. doi:10.1038/s43247-022-00606-3.

Gusman, A.R., Roger, J., Noble, C., Wang, X., Power, W., Burbidge, D., 2022. The 2022 Hunga Tonga-Hunga Ha'apai Volcano Air-Wave Generated Tsunami. Pure and Applied Geophysics 179, 3511–3525. doi:10.1007/s00024-022-03154-1.

Hunter, J.D., 2007. Matplotlib: A 2d graphics environment. Computing in Science Engineering 9, 90–95. doi:10.1109/MCSE.2007.55.

Iezzi, A.M., Matoza, R.S., Bishop, J.W., Bhetanabhotla, S., Fee, D., 2022. Narrow-band least-squares infrasound array processing. Seismological Research Letters 93, 2818–2833. doi:10.1785/0220220042.

Jarvis, P.A., Caldwell, T.G., Noble, C., Ogawa, Y., Vagasky, C., 2024. Volcanic lightning reveals umbrella cloud dynamics of the 15 January

2022 Hunga volcano eruption, Tonga. Bulletin of Volcanology 86, 54. doi:10.1007/s00445-024-01739-3.

Kintner, J.A., Yeck, W.L., Earle, P.S., Prejean, S., Pesicek, D., 2022. High-Precision Characterization of Seismicity from the 2022 Hunga Tonga-Hunga Ha'apai Volcanic Eruption. Seismological Research Letters , 14.

Kraft, T., Ling, O.K.A., Toledo, T., Scheu, B., Stähler, S.C., Clinton, J., Stange, S., 2023. An Antipodal Seismic and (Infra)acoustic View from Central Europe on the 15 January 2022 Hunga–Tonga–Hunga–Ha'apai Eruption. Seismological Research Letters doi:10.1785/0220220254.

Krischer, L., Megies, T., Barsch, R., Beyreuther, M., Lecocq, T., Caudron, C., Wassermann, J., 2015. ObsPy: a bridge for seismology into the scientific Python ecosystem. Computational Science Discovery 8, 1–17. doi:10.1088/1749-4699/8/1/014003.

Kubota, T., Saito, T., Nishida, K., 2022. Global fast-traveling tsunamis driven by atmospheric Lamb waves on the 2022 Tonga eruption. Science 377, 91–94. doi:10.1126/science.abo4364.

Lawson, R., Potter, S.H., Harrison, S., Clark, K., Clive, M., Charlton, D., Burbidge, D., Kilgour, G.N., 2022. Crowdsourced tsunami and sound observations in Aotearoa New Zealand following the Hunga Tonga-Hunga Ha'apai (HTHH) eruption on 15 January 2022 doi:10.21420/6JXP-RM04.

Le Bras, R.J., Zampolli, M., Metz, D., Haralabus, G., Bittner, P., Villarroel, M., Matsumoto, H., Graham, G., Meral Özel, N., 2022. The Hunga Tonga–Hunga Ha'apai Eruption of 15 January 2022: Observations on the

International Monitoring System (IMS) Hydroacoustic Stations and Synergy with Seismic and Infrasound Sensors. Seismological Research Letters doi:10.1785/0220220240.

Le Pichon, A., Blanc, E., Hauchecorne, A. (Eds.), 2019. Infrasound Monitoring for Atmospheric Studies: Challenges in Middle Atmosphere Dynamics and Societal Benefits. Springer International Publishing. doi:10.1007/978-3-319-75140-5.

Lynett, P., McCann, M., Zhou, Z., Renteria, W., Borrero, J., Greer, D., Fa'anunu, O., Bosserelle, C., Jaffe, B., La Selle, S., Ritchie, A., Snyder, A., Nasr, B., Bott, J., Graehl, N., Synolakis, C., Ebrahimi, B., Cinar, G.E., 2022. Diverse tsunamigenesis triggered by the Hunga Tonga-Hunga Ha'apai eruption. Nature 609, 728–733. doi:10.1038/s41586-022-05170-6.

Mastin, L.G., Van Eaton, A.R., Cronin, S.J., 2024. Did steam boost the height and growth rate of the giant Hunga eruption plume? Bulletin of Volcanology 86, 64. doi:10.1007/s00445-024-01749-1.

Matoza, R.S., Fee, D., Assink, J.D., Iezzi, A.M., Green, D.N., Kim, K., Toney, L., Lecocq, T., Krishnamoorthy, S., Lalande, J.M., Nishida, K., Gee, K.L., Haney, M.M., Ortiz, H.D., Brissaud, Q., Martire, L., Rolland, L., Vergados, P., Nippress, A., Park, J., Shani-Kadmiel, S., Witsil, A., Arrowsmith, S., Caudron, C., Watada, S., Perttu, A.B., Taisne, B., Mialle, P., Le Pichon, A., Vergoz, J., Hupe, P., Blom, P.S., Waxler, R., De Angelis, S., Snively, J.B., Ringler, A.T., Anthony, R.E., Jolly, A.D., Kilgour, G., Averbuch, G., Ripepe, M., Ichihara, M., Arciniega-Ceballos, A., Astafyeva, E., Ceranna, L., Cevuard, S., Che, I.Y., De Negri, R., Ebeling, C.W., Evers, L.G., Franco-Marin, L.E., Gabrielson, T.B., Hafner, K., Harrison, R.G., Komjathy, A., Lacanna, G., Lyons, J., Macpherson, K.A., Marchetti, E., McKee, K.F., Mellors, R.J., Mendo-Pérez, G., Mikesell, T.D., Munaibari, E., Oyola-Merced, M., Park, I., Pilger, C., Ramos, C., Ruiz, M.C., Sabatini, R., Schwaiger, H.F., Tailpied, D., Talmadge, C., Vidot, J., Webster, J., Wilson, D.C., 2022. Atmospheric waves and global seismoacoustic observations of the January 2022 Hunga eruption, Tonga. Science 377, 95–100. doi:10.1126/science.abo7063.

Matoza, R.S., Hedlin, M.A., Garcés, M.A., 2007. An infrasound array study of mount st. helens. Journal of Volcanology and Geothermal Research 160, 249–262. doi:10.1016/j.jvolgeores.2006.10.006.

McKee, K., Fee, D., Haney, M.M., Matoza, R.S., Lyons, J., 2018. Infrasound signal detection and back-azimuth estimation using ground-coupled airwaves on a seismo-acoustic sensor pair. Journal of Geophysical Research: Solid Earth doi:10.1029/2017JB015132.

Nozuka, Y., Inchin, P.A., Kaneko, Y., Sabatini, R., Snively, J.B., 2024. Earthquake source impacts on the generation and propagation of seismic infrasound to the upper atmosphere. Geophysical Journal International 238, 537–556. doi:10.1093/gji/ggae170.

Ohya, H., Tsuchiya, F., Takamura, T., Shinagawa, H., Takahashi, Y., Chen, A.B., 2024. Lower ionospheric resonance caused by Pekeris wave induced by 2022 Tonga volcanic eruption. Scientific Reports 14, 15659. doi:10.1038/s41598-024-65929-x.

Pekeris, C., 1937. Atmospheric oscillations. Proceedings of the Royal Society of London. Series A - Mathematical and Physical Sciences 158, 650–671. doi:10.1098/rspa.1937.0046.

Petersen, T., Gledhill, K., Chadwick, M., Gale, N.H., Ristau, J., 2011. The New Zealand National Seismograph Network. Seismological Research Letters 82, 9–20. doi:10.1785/gssrl.82.1.9.

Podglajen, A., Le Pichon, A., Garcia, R.F., Gérier, S., Millet, C., Bedka, K., Khlopenkov, K., Khaykin, S., Hertzog, A., 2022. Stratospheric Balloon Observations of Infrasound Waves From the 15 January 2022 Hunga Eruption, Tonga. Geophysical Research Letters 49. doi:10.1029/2022GL100833.

Poli, P., Shapiro, N.M., 2022. Rapid Characterization of Large Volcanic Eruptions: Measuring the Impulse of the Hunga Tonga Ha'apai Explosion From Teleseismic Waves. Geophysical Research Letters 49. doi:10.1029/2022GL098123.

Proud, S.R., Prata, A.T., Schmauß, S., 2022. The January 2022 eruption of Hunga Tonga-Hunga Ha'apai volcano reached the mesosphere, volume=378, issn=0036-8075, 1095-9203. Science , 554–557doi:10.1126/science.abo4076.

Purkis, S.J., Ward, S.N., Fitzpatrick, N.M., Garvin, J.B., Slayback, D., Cronin, S.J., Palaseanu-Lovejoy, M., Dempsey, A., 2023. The 2022 Hunga-Tonga megatsunami: Near-field simulation of a once-in-a-century event. Science Advances 9, eadf5493. doi:10.1126/sciadv.adf5493.

Raspberry Shake, S.A., 2016. Raspberry shake. URL: https://www.fdsn.org/networks/detail/AM/, doi:10.7914/SN/AM.

Reed, J.W., 1987. Air pressure waves from Mount St. Helens eruptions. Journal of Geophysical Research 92, 11979. doi:10.1029/JD092iD10p11979.

Ripepe, M., Marchetti, E., 2002. Array tracking of infrasonic sources at Stromboli volcano. Geophysical Research Letters 29, 33–1–33–4. doi:10.1029/2002GL015452.

Strachey, R., 1888. On the air waves and sounds caused by the eruption of Krakatoa in August 1883. Trübner & Co. p. 78–88.

Szuberla, C.A.L., Arnoult, K.M., Olson, J.V., 2006. Discrimination of near-field infrasound sources based on time-difference of arrival information. The Journal of the Acoustical Society of America 120, EL23–EL28. doi:10.1121/1.2234517.

Thurin, J., Tape, C., 2023. Comparison of force and moment tensor estimations of subevents during the 2022 Hunga-Tonga submarine volcanic eruption. Geophysical Journal International , ggad323doi:10.1093/gji/ggad323.

Thurin, J., Tape, C., Modrak, R., 2022. Multi-Event Explosive Seismic Source for the 2022 Mw 6.3 Hunga Tonga Submarine Volcanic Eruption. The Seismic Record 2, 217–226. doi:10.1785/0320220027.

Uieda, L., Tian, D., Leong, W.J., Schlitzer, W., Grund, M., Jones, M., Fröhlich, Y., Toney, L., Yao, J., Magen, Y., Tong, J.H., Materna, K., Belem, A., Newton, T., Anant, A., Ziebarth, M., Quinn, J., Wessel, P., 2023. PyGMT: A Python interface for the Generic Mapping Tools. URL: https://doi.org/10.5281/zenodo.7772533, doi:10.5281/zenodo.7772533.

Van Eaton, A.R., Lapierre, J., Behnke, S.A., Vagasky, C., Schultz, C.J., Pavolonis, M., Bedka, K., Khlopenkov, K., 2023. Lightning Rings and Gravity Waves: Insights Into the Giant Eruption Plume From Tonga's Hunga Volcano on 15 January 2022. Geophysical Research Letters 50, e2022GL102341. doi:10.1029/2022GL102341.

Vergoz, J., Hupe, P., Listowski, C., Le Pichon, A., Garcés, M.A., Marchetti, E., Labazuy, P., Ceranna, L., Pilger, C., Gaebler, P., Näsholm, S., Brissaud, Q., Poli, P., Shapiro, N., De Negri, R., Mialle, P., 2022. IMS observations of infrasound and acoustic-gravity waves produced by the January 2022 volcanic eruption of Hunga, Tonga: A global analysis. Earth and Planetary Science Letters 591, 13. doi:10.1016/j.epsl.2022.117639.

Watanabe, S., Hamilton, K., Sakazaki, T., Nakano, M., 2022. First Detection of the Pekeris Internal Global Atmospheric Resonance: Evidence from the 2022 Tonga Eruption and from Global Reanalysis Data. Journal of the Atmospheric Sciences 79, 3027–3043. doi:10.1175/JAS-D-22-0078.1.

Withers, M., Aster, R.C., Young, C.J., Beiriger, J., Harris, M., Moore, S., Trujillo, J., 1998. A comparison of select trigger algorithms for automated global seismic phase and event detection. Bulletin of the Seismological Society of America 88, 95–106.

Wright, C.J., Hindley, N.P., Alexander, M.J., Barlow, M., Hoffmann, L., Mitchell, C.N., Prata, F., Bouillon, M., Carstens, J., Clerbaux, C., Osprey, S.M., Powell, N., Randall, C.E., Yue, J., 2022. Surface-to-space atmospheric waves from Hunga Tonga–Hunga Ha'apai eruption. Nature 609, 741–746. doi:10.1038/s41586-022-05012-5.

Supplementary material for: Audible and Infrasonic waves generated during the 2022 Hunga eruption: Observations from across Aotearoa New Zealand

Oliver D. Lamb, Paul Jarvis, Geoff Kilgour

August 8, 2024

Band	Frequency range [Hz]	Window length [s]
1	0.001 – 0.002	2400
2	0.002 – 0.004	2082
3	0.004 – 0.008	1765
4	0.008 – 0.016	1448
5	0.016 – 0.032	1131
6	0.032 – 0.063	814
7	0.063 – 0.125	497
8	0.125 – 0.250	180

Table S1: Details of windows used for narrow-band least squares array processing

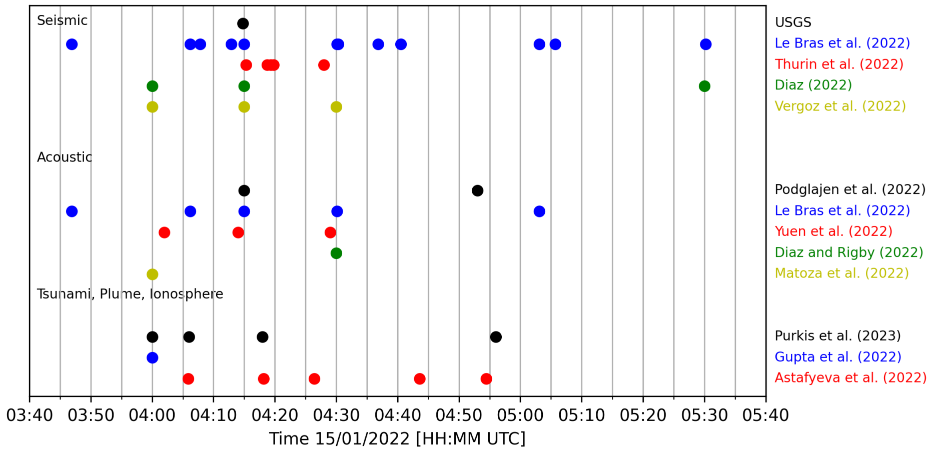

Figure S1: Illustration of eruption timelines from different investigations, where each dot indicates the time of an event identified by the investigators. The references for each investigation are indicated on the right.

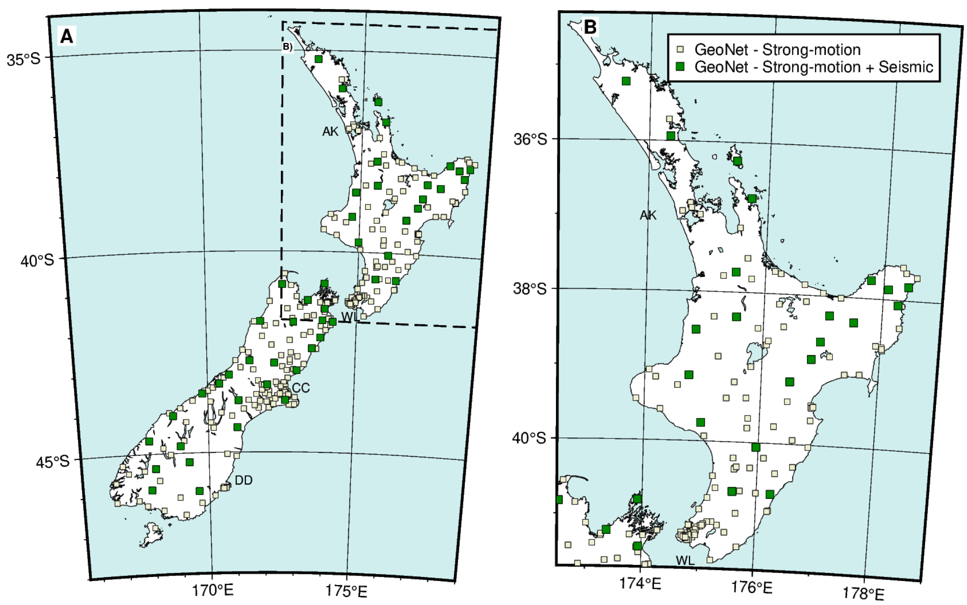

Figure S2: Map of Aotearoa New Zealand showing locations of strong-motion accelerometers co-located with seismometers used for STA/LTA analysis in this study (green squares). Also plotted are the locations of other GeoNet stong-motion accelerometers that were operating on 15 January 2022 but were not used for this study (light yellow squares).

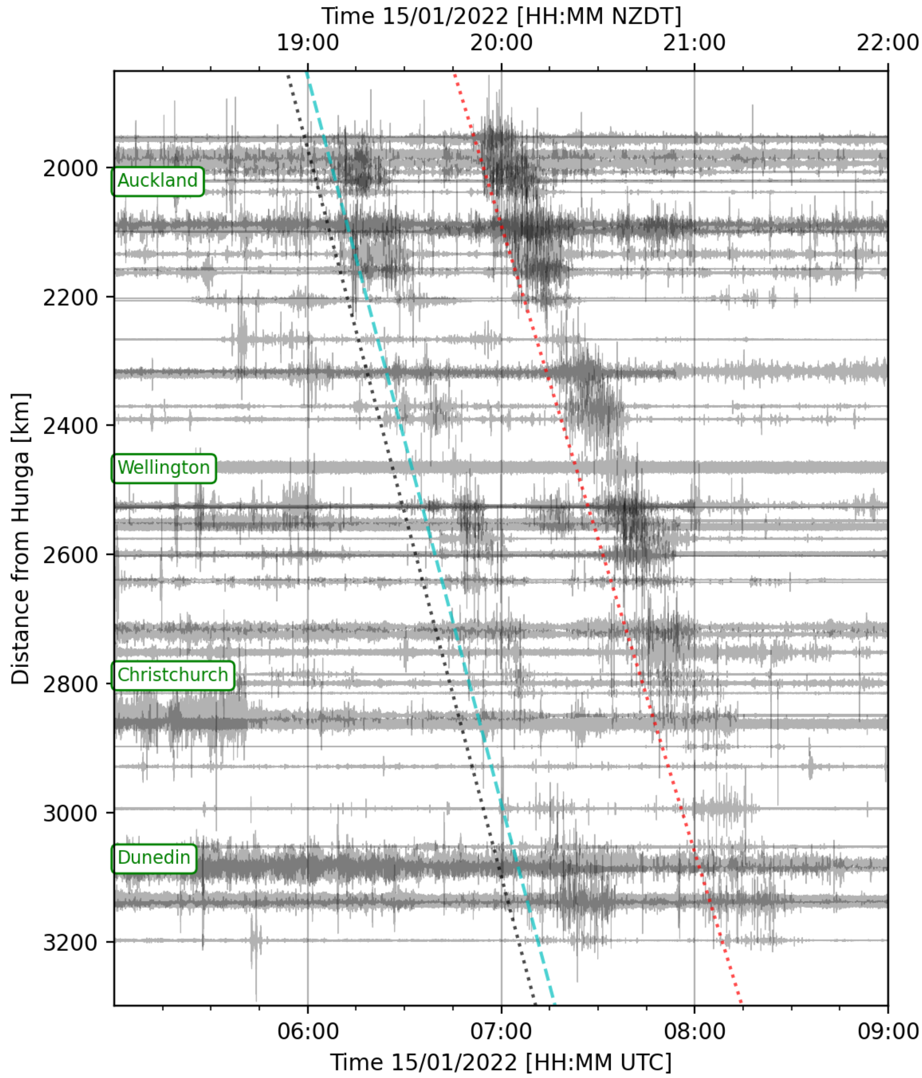

Figure S3: Data from strong-motion accelerometers co-located with seismometers in the GeoNet network as recorded on 15 January 2022. Also plotted are arrival times for the Lamb wave (black dotted line), and audible wavepackets 1 and 2 (cyan dashed and red dot-dash line), and distances of major cities in Aotearoa New Zealand.

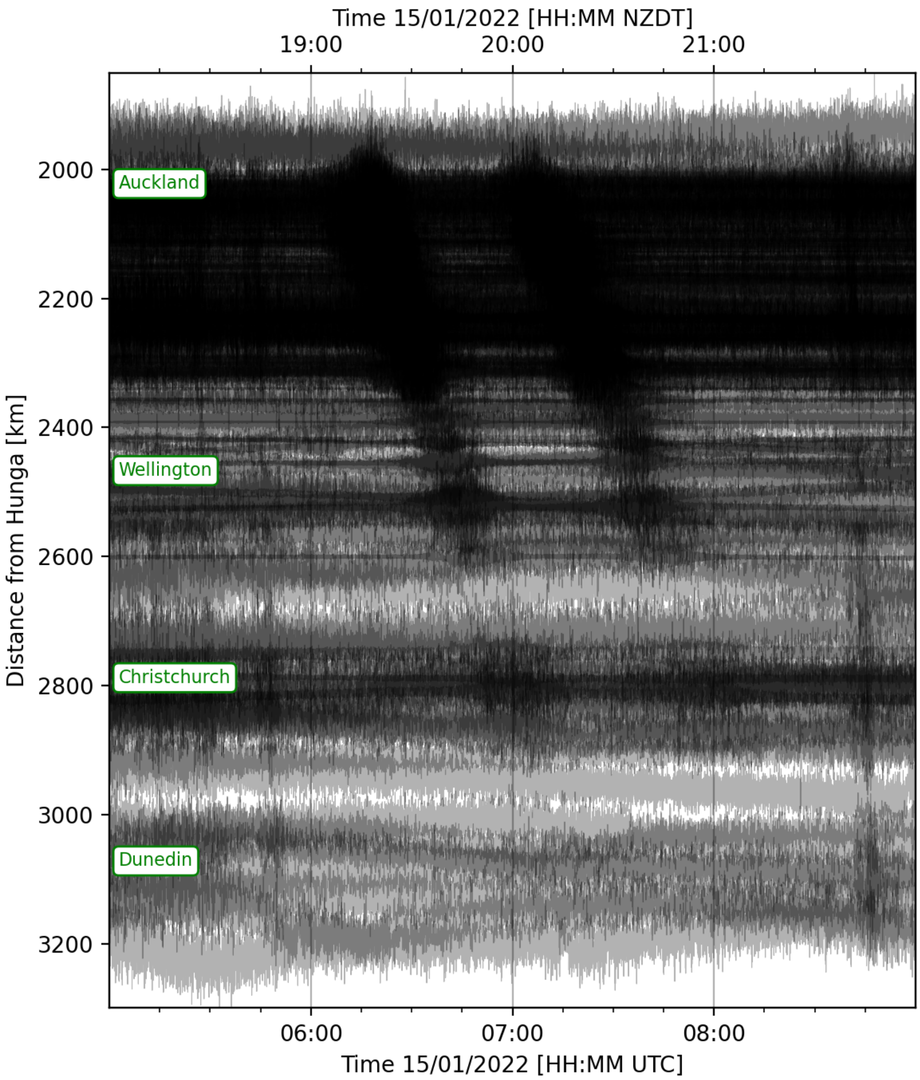

Figure S4: Unfiltered seismic data recorded across Aotearoa New Zealand after the Hunga eruption on 15 January 2022, highpass filtered at 20 Hz. Also plotted are distances of major cities in Aotearoa New Zealand.

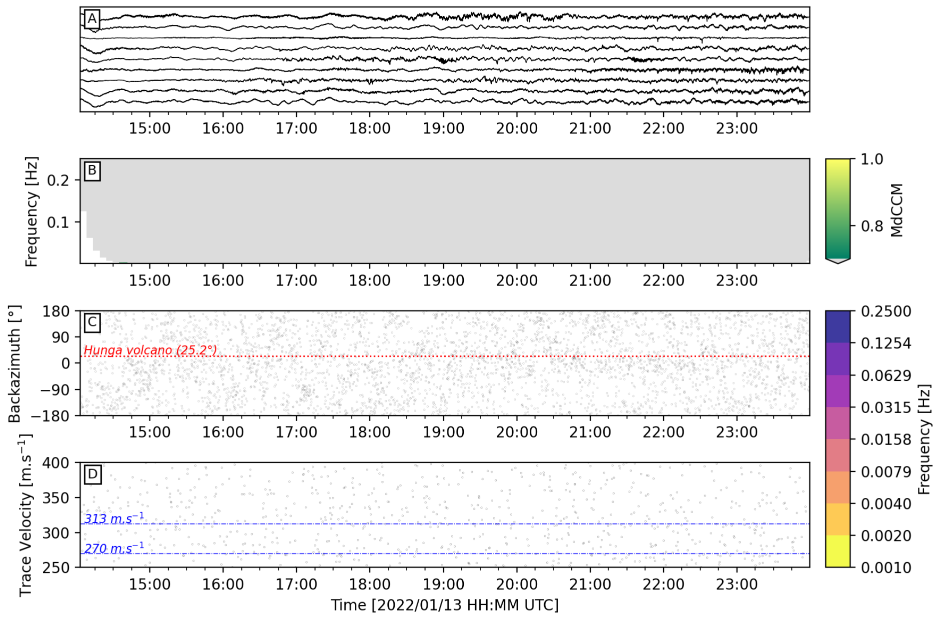

Figure S5: Results of array processing using microphones around the Tongariro-Ngauruhoe volcanoes for 13 January 2022. (A) Acoustic data as recorded by the stations used in the array processing, bandpass filtered at 0.001 to 0.25 Hz. (B) MdCCM for each time window and frequency band; estimations below the 0.7 threshold are coloured in grey. Each estimate is plotted at the end of their respective time window. (C) Back-azimuth and (D) Trace velocity estimates for MdCCM >0.7 and σ_τ <1, coloured by frequency. Estimates which fall outside those thresholds are plotted as grey dots.

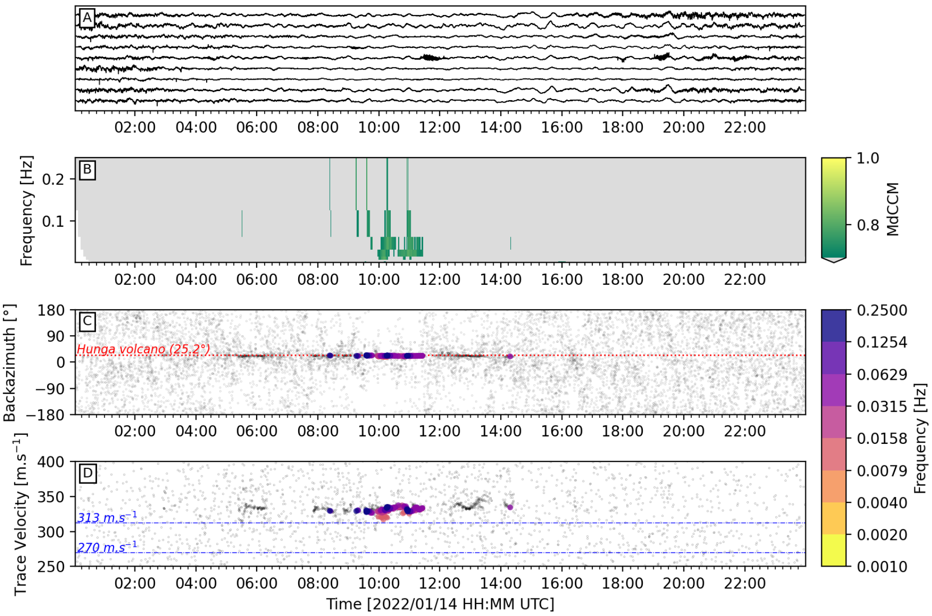

Figure S6: Results of array processing using microphones around the Tongariro-Ngauruhoe volcanoes for 14 January 2022. See caption for Fig. S5 for explanation of panels.